Tropical Cells and a Secondary Circulation near the Northern Front of the Equatorial Pacific Cold Tongue*

RENELLYS C. PEREZ

Cooperative Institute for Marine and Atmospheric Studies, University of Miami, and National Oceanic and Atmospheric Administration/Atlantic Oceanographic and Meteorological Laboratory, Miami, Florida

MEGHAN F. CRONIN AND WILLIAM S. KESSLER

National Oceanic and Atmospheric Administration/Pacific Marine Environmental Laboratory, Seattle, Washington

(Manuscript received 22 September 2009, in final form 20 April 2010)

ABSTRACT

Shipboard measurements and a model are used to describe the mean structure of meridional–vertical tropical cells (TCs) in the central equatorial Pacific and a secondary circulation associated with the northern front of the cold tongue. The shape of the front is convoluted by the passage of tropical instability waves (TIWs). When velocities are averaged in a coordinate system centered on the instantaneous position of the northern front, the measurements show a near-surface minimum in northward flow north of the surface front (convergent flow near the front). This convergence and inferred downwelling extend below the surface mixed layer, tilt poleward with depth, and are meridionally bounded by regions of divergence and upwelling. Similarly, the model shows that, on average, surface cold tongue water moves northward toward the frontal region and dives below tilted front, whereas subsurface water north of the front moves southward toward the front, upwells, and then moves northward in the surface mixed layer. The model is used to demonstrate that this mean quasi-adiabatic secondary circulation is not a frozen field that migrates with the front but is instead highly dependent on the phase of the TIWs: southward-upwelling flow on the warm side of the front tends to occur when the front is displaced southward, whereas northward-downwelling flow on the cold side of the front occurs when the front is displaced northward. Consequently, when averaged in geographic coordinates, the observed and simulated TCs appear to be equatorially asymmetric and show little trace of a secondary circulation near the mean front.

1. Introduction

There are few direct estimates of the mean structure of meridional and vertical currents in the central equatorial Pacific Ocean (defined here as region bounded by 8°S–8°N, 140°–125°W). To date, the best observational representation comes from 9 years of shipboard acoustic Doppler current profiler (ADCP) transects collected between 170° and 95°W (Johnson et al. 2001, hereafter JMF01). These shipboard observations show evidence of shallow tropical cells (TCs) characterized by equatorial upwelling, poleward Ekman flow in the surface mixed layer, off-equatorial downwelling within 8° latitude of the equator, and equatorward geostrophic flow below the mixed layer (Fig. 1). The TCs appear as near-surface, near-equatorial maxima of the much larger subtropical cells (McCreary and Lu 1994) and are embedded in strong westward and eastward flows, with the northern TC appearing to be stronger (JMF01). When temporally averaged in depth coordinates, numerical models show similar shallow cells (McCreary 1981; Philander et al. 1987; Kessler et al. 1998; Lu et al. 1998; Hazeleger et al. 2001; Izumo 2005; Brown et al. 2007a,b; Perez and Kessler 2009). However, when averaged in isopycnal coordinates, the mean TCs in models virtually disappear, implying off-equatorial downwelling may be due to averaging an adiabatic three-dimensional flow across the sloping density surfaces associated with the cold tongue

* Pacific Marine Environmental Laboratory Contribution Number 3300.

Corresponding author address: Renellys C. Perez, Cooperative Institute for Marine and Atmospheric Studies, University of Miami, 4600 Rickenbacker Causeway, Miami, FL 33149.
E-mail: renellys.c.perez@noaa.gov

DOI: 10.1175/2010JPO4366.1

© 2010 American Meteorological Society

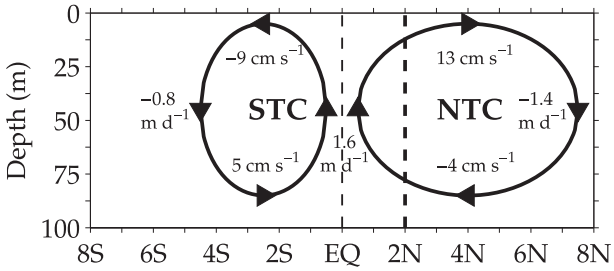

FIG. 1. Schematic of meridional–vertical structure of the TCs in the central and eastern equatorial Pacific following JMF01. The southern TC (STC) and northern TC (NTC) are labeled. Dashed line at 2°N depicts approximate position of the northern front of the cold tongue.

fronts (Hazeleger et al. 2001; Brown et al. 2007b; Richards et al. 2009). In this analysis, we reprocess an extended shipboard ADCP dataset collected in the central equatorial Pacific to highlight and better understand the circulation near the strong northern front of the cold tongue. Results from a 9-yr tropical Pacific model simulation are used to interpret the shipboard observations.

The presence of a strong front bounding the equatorial cold tongue at its northern edge near 2°N in the mean (Wallace et al. 1989) complicates the simple depiction of the TCs given by Fig. 1. The front persists as a sharp gradient for months, which implies that northward-moving cold water on the southern side cannot directly cross it, because there is no apparent mechanism to warm the water parcels rapidly. One possibility is that the cold, northward-moving water slides under the warm water to the north. Then both water masses could be flowing north at the surface (satisfying the constraint of poleward Ekman flow), and the front would be associated with quasi-adiabatic downwelling on its southern (i.e., cold) side and corresponding upwelling on its northern (i.e., warm) side to replenish northward surface flow.

Such slantwise motion along a two-dimensional front can occur for a number of dynamical reasons. In the presence of geostrophic wind shear, slantwise convection can occur along tilted absolute momentum surfaces during symmetric (hybrid gravitational–centrifugal) instability (e.g., Haine and Marshall 1998; Straneo et al. 2002). Slantwise motion can also occur as an Ekman response to friction acting on the geostrophic shear associated with a front (Garrett and Loder 1981; Thompson 2000) and can still exist when winds blow along the front (Thomas and Ferrari 2008). Cronin and Kessler (2009, hereafter CK09), using 9 months of current meter data in the upper 25 m at 2°N, 140°W, found that, in the case of the northern front of the cold tongue and strong easterly (alongfront) trade winds, the geostrophic shear tends to modify the ageostrophic Ekman spiral and reduce the expected near-surface poleward Ekman flow at the front. These observations suggest that there is convergence of meridional flow on the cold side of the front and divergence of meridional flow on the warm side of the front.

Moreover, the cold tongue has significant intraseasonal-to-interannual variability, and its northern front cannot be viewed as a static two-dimensional front. The cold tongue and front are weak during El Niño warm events and strong during La Niña cold events (Wallace et al. 1989; Deser and Wallace 1990). Likewise, the front is weak during the warm season from March through May when the cold tongue has receded and gradually sharpens from July through November when the cold tongue extends westward to the central Pacific (Wallace et al. 1989; Deser and Wallace 1990; Mitchell and Wallace 1992). When the front is fully formed, it also has significant variability associated with tropical instability waves (TIWs; Baturin and Niiler 1997; Kessler et al. 1998; Contreras 2002; Lyman et al. 2007). TIWs distort the front into cusplike wave patterns with 15–40-day periods (Qiao and Weisberg 1995; Lyman et al. 2007, and references therein), zonal wavelengths on the order of 1000 km (Legeckis 1977; Qiao and Weisberg 1995), and westward phase speeds between 0.3 and 0.6 m s^{-1} (Qiao and Weisberg 1995). Many modeling and observational studies have described the large-amplitude meridional and vertical motion associated with Northern Hemisphere TIWs and tropical instability vortices (TIVs) in both the Pacific and Atlantic Oceans (Philander et al. 1986; Flament et al. 1996; Johnson 1996, Kennan and Flament 2000; Menkes et al. 2002, 2006; Jochum and Murtugudde 2006; Dutrieux et al. 2008; CK09). These studies document instances of convergent flow and downwelling on the western side of the TIW cusps (leading edges of the TIW cusps) and divergent flow and upwelling on the eastern side of the TIW cusps (trailing edges of the TIW cusps) but do not explore the mean impact of these waves and vortices on the circulation near the front.

The shape of the northern front is strongly convoluted by the passage of TIWs, undulating up to 5° latitude away from the mean position of the front (e.g., Flament et al. 1996; Kennan and Flament 2000), and the front and frontal processes are therefore significantly reduced when averaged over time in fixed geographic coordinates. The question we address is whether the instantaneous front is associated with a quasi-adiabatic secondary circulation and whether this frontal circulation is manifest when averaged in time over many TIWs and seasons. In this study, we map the flow in a coordinate system centered on the instantaneous position of the northern front of the cold tongue (frontal coordinates) to highlight the large meridional and vertical motion associated with the front in the upper 100 m of the water column. This is an

alternative to isopycnal coordinate mapping, which requires collocated density and velocity profiles and an often aphysical matching between the flow in the surface mixed layer and the flow in the stratified density layers beneath the surface mixed layer [e.g., Johnson et al. (2002) applied a shape-preserving spline]. The paper outline is as follows: A description of the data and model simulation is provided in section 2. Details of the frontal coordinate transformation are given in section 3. In section 4, the mean structure of temperature, horizontal currents, divergence of meridional flow, and vertical currents are described in both geographic and frontal coordinates. Section 4 also explores how the frontal circulation varies with the phase of the TIWs. Results are discussed and summarized in section 5.

2. Data and numerical model

a. Shipboard and satellite data

Shipboard ADCP latitude and depth (y, z) transects collected while servicing the Tropical Atmosphere Ocean (TAO) mooring array provide direct quasi-synoptic measurements of horizontal velocity in the equatorial Pacific (Johnson and Plimpton 1999; JMF01). Our study focuses on all TAO transects collected between November 1991 and February 2008 along two adjacent TAO meridians in the central equatorial Pacific, 140° and 125°W. Data from individual TAO cruises are made available through the Joint Archive for Shipboard ADCP (JASADCP), a National Oceanic and Atmospheric Administration (NOAA) and University of Hawaii at Manoa (UH) collaboration. These quality-controlled gridded datasets contain hourly velocities interpolated to 10-m depth intervals starting at 20-m depth. Transmit frequency and instrument configuration of the ADCP dictate the depth of the shallowest bin, width of vertical bins, and vertical extent of the measurements. Early TAO shipboard ADCP measurements were made with a transmit frequency of 150 kHz, a bin length of 8 m, and a nominal depth range of 16–472 m. In 2004, a transition was made to an ADCP with 75-kHz transmit frequency, doubling the bin length to 16 m and increasing the nominal depth range (29–973 m). In 2006, the depth of the shallowest bin was shifted from 29 m down to 37 m. Therefore, 40 m is the shallowest depth that every transect resolves (67% and 84% of the transects resolve flow at 20 and 30 m, respectively). CK09 found that the vertical shear of near-surface horizontal currents at 2°N, 140°W depends on the viscosity profile, wind stress, and buoyancy gradient. Because these are not necessarily known in the central equatorial Pacific, we refrain from extrapolating shipboard ADCP velocities to fill in the unmeasured currents in the downward-looking shipboard ADCP "blind spot" (as in JMF01). Instead, output from the simulation described in section 2b is used to put the observed means at 20 m into context.

Temperature measurements, made by a thermistor at the ADCP transducer head (nominal depth of 5 m) for sound speed correction (Johnson and Plimpton 1999), are used to identify the center of the northern front of the cold tongue. When available, two gridded SST products obtained from the UH Asia-Pacific Data-Research Center (APDRC) public data server are used to fill gaps in the transducer temperature data. The first product blends NOAA/National Climatic Data Center (NCDC) daily high-resolution SST with Advanced Very High Resolution Radiometer (AVHRR) SST observations via optimum interpolation (OI; referred to as NOAA/OI SST; Reynolds et al. 2007). NOAA/OI SST is globally available from January 1985 to September 2007 on a 0.25° grid. The second product is 3-day running mean SST from the Tropical Rainfall Measuring Mission (TRMM) Microwave Imager (TMI SST; Kummerow et al. 1998). TMI SST is available from December 1997 to February 2008 with resolution of 0.25° between 40°S and 40°N.

b. Numerical model

Daily averages from a Modular Ocean Model (MOM4; Griffies et al. 2003) simulation in the tropical Pacific forced with monthly mean Quick Scatterometer (QuikSCAT) wind stress from September 1999 to August 2008 are used to interpret the shipboard observations. The model was initially spun up over a 20-yr period with QuikSCAT climatological wind stress (Risien and Chelton 2008), turbulent surface fluxes from Massachusetts Institute of Technology (MIT)–Woods Hole Oceanographic Institute (WHOI) objectively analyzed air–sea fluxes (OAFlux; Yu et al. 2004; Yu and Weller 2007), and longwave and shortwave radiation from the International Satellite Cloud Climatology Project (ISCCP; Zhang et al. 2004). The resolution of the model in the equatorial waveguide is 0.33° latitude by 0.625° longitude, and there are 49 z levels with 10-m resolution in the upper 220 m of the water column.

Additional details on the climatologically driven model simulation can be found in Perez and Kessler (2009). They compared the mean model TCs along 140°W from year 17 of the simulation against the JMF01 observed means (see their Fig. 1). The model and observed zonal and meridional currents agreed well, with upwelling (downwelling) largely controlled by the divergence (convergence) of the meridional flow. On closer inspection of the mean TCs, however, the model meridional and vertical currents were more asymmetric than observed with faster flow in the surface and subsurface limb of the northern TC. The model also produced paired equatorial

TABLE 1. Comparison of transducer temperature and gridded SST products.

Transect	Bias (°C)	Correlation
	NOAA/OI SST	
140°W	0.39 ± 0.16	0.89 ± 0.03
125°W	0.44 ± 0.18	0.92 ± 0.03
	TMI SST	
140°W	0.71 ± 0.10	0.91 ± 0.03
125°W	0.75 ± 0.07	0.96 ± 0.01

upwelling maxima near 1°S and 1°N rather than a single maximum centered on the equator. Given the considerable spatiotemporal averaging of the JMF01 observed means, the strength of the equatorial asymmetry and the existence of paired equatorial upwelling maxima could not be confirmed or rejected. Thus, an updated description of the observed means in the central equatorial Pacific Ocean is needed, specifically one that highlights how the flow is modified in the vicinity of the northern front of the cold tongue.

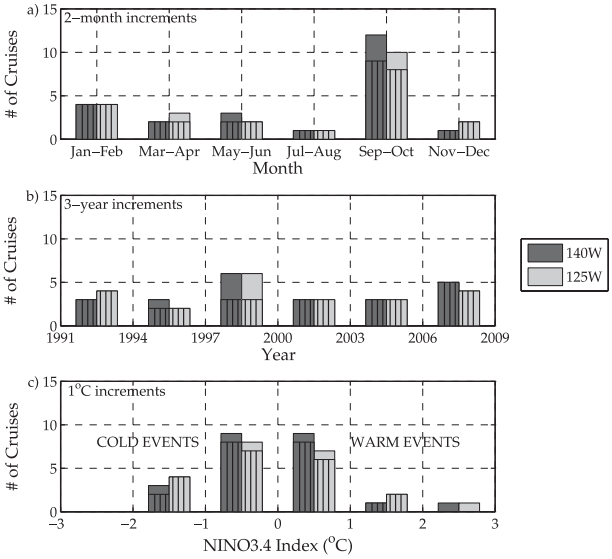

FIG. 2. Number of observations included in averages along TAO meridians, 140° and 125°W. Histograms are binned by (a) 2-month increments, (b) 3-yr increments, and (c) 1°C increments of the ENSO Niño-3.4 temperature anomaly index. The stippled shading indicates number of observations included in frontal mean calculation.

3. Methodology

In all, 45 full (8°S–8°N) or partial ADCP transects were used to compute the observed means (23 and 22 transects along 140° and 125°W, respectively). We zonally averaged data collected along 140° and 125°W to decrease the sampling errors (section 3b). These adjacent transects were typically surveyed in the same cruise separated by a week in time (JMF01), and when TIWs are present, captured two different TIW phases. Hence, zonal averaging also reduced aliasing by TIWs. Because the difference in the depth of the mean TCs between 140° and 125°W is typically small (less than 10 m), these two meridians can be averaged together.

For each cruise transect, near-surface (5 m) temperature and horizontal velocity measurements between 8°S and 8°N and within 1° longitude of the meridian were objectively mapped onto a 0.05° latitude grid assuming a Gaussian covariance (Bretherton et al. 1976) and using a meridional correlation length scale of 2° latitude and a noise-to-signal energy ratio of 0.01 (similar to values used by JMF01, 1° and 0.01, respectively). This removed small-meridional-scale variations in the data due to extended periods on station and put irregularly spaced data onto a uniform latitudinal grid.

Transducer temperature data were sometimes missing or incomplete along a transect, and NOAA/OI SST and TMI SST were used to fill in these gaps (see section 2a). In practice, the gridded products were averaged for the duration of each transect, adjusted for mean transect biases (because of the difference between SST and 5-m temperatures and sampling differences), and then combined with transducer data prior to objective mapping. Table 1 shows the mean biases and correlations between transducer temperature and NOAA/OI SST and transducer temperature and TMI SST, respectively, in the central equatorial Pacific. The transducer temperature was approximately 0.4°C warmer than NOAA/OI SST and approximately 0.7°C warmer than TMI SST. Both TMI SST and NOAA/OI SST were well correlated with the transducer temperature (greater than 0.89) and were therefore suitable for filling in data gaps.

Although 45 transects were used to compute the geographic means, 7 transects were discarded from the frontal mean calculation (frontal coordinates described in section 3b). Four of the discarded transects were not included because they were obtained during extreme warm anomalies of the 1997/98 El Niño when the center of the northern front of the cold tongue could not be clearly identified. The other three transects were discarded because the center of the cold tongue was located south of the equator.

a. Distribution of cruises

Although the TAO meridians were ostensibly sampled every 6 months (Johnson and Plimpton 1999), the distribution of the cruises show a strong seasonal bias with September–October, the most heavily sampled 2-month period (Fig. 2a). The fall bias, first noted in

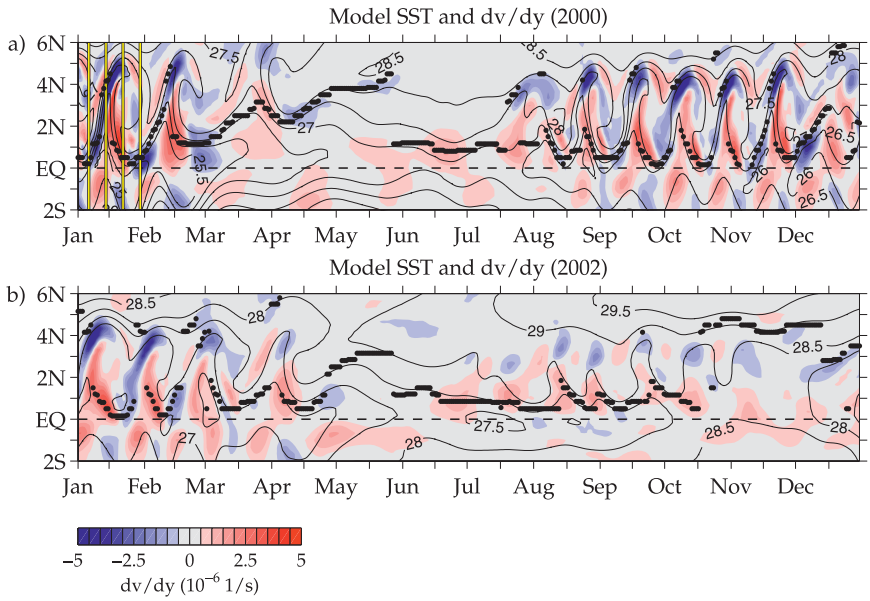

FIG. 3. Meridional–temporal structure of the model near-surface meridional divergence (averaged from 20- to 40-m depth) along 140°W in years (a) 2000 and (b) 2002 with near-surface (5 m) temperature contours and front positions overlaid as black dots. Yellow lines in (a) identify transects that relate to Fig. 12.

JMF01, favored months of the year when the cold tongue was well defined and TIWs were growing in amplitude (e.g., seasonal cold bias). There are samples collected during every 2-month period, with the fewest samples collected in July–August (Fig. 2a). The majority of the transects withheld from the frontal mean calculation were collected in September–October (unstippled shading in Fig. 2a).

The most heavily sampled periods were 1997–99 and 2006–08; however, the majority of the transects removed from the frontal mean calculation was collected during the 1997/98 El Niño (cf. stippled and unstippled shading in Fig. 2b). There were few measurements available from the early 2000s because of an uncorrectable 1°–2° bearing error on instruments aboard the NOAA ship *Ka'imimoana* from February 2001 to February 2004 (J. Hummon 2008, personal communication). The compass-error-contaminated velocity measurements were excluded from this analysis.

Figure 2c identifies whether samples were collected during anomalously warm (El Niño) or anomalously cold (La Niña) periods, as defined by the value of the Niño-3.4 anomaly during the month of each cruise. Positive and negative anomalies with magnitudes between 0° and 1°C indicate relatively mild warm and cold events, respectively. The majority of samples used in the frontal mean calculation were collected during mild cold events, with a negligible cold bias of $-0.09° \pm 0.14°C$. The cold bias was partly due to excluding data collected during the 1997/98 El Niño (unstippled shading in Figs. 2b,c). The geographic means that were computed from all 45 transects have a negligible warm bias of $0.03° \pm 0.15°C$.

b. *Identification of front and frontal coordinate system*

To resolve important frontal processes lost by averaging in geographic coordinates and determine whether the front is associated with a quasi-adiabatic secondary circulation, we portray the data in a frontal coordinate system (coordinates centered on the instantaneous position of the northern front of the cold tongue). To do this, for each transect we defined the center of the northern front of the cold tongue θ_c as the latitude of the largest meridional temperature gradient between the cold tongue minimum (θ_1, latitude of coldest temperature between 2°S and 5°N) and the edge of the northern front (θ_2, latitude of first zero crossing of meridional temperature gradient north of θ_1). This approach produces a composite front that is sharp, similar to the instantaneous expression. Figure 3 demonstrates how much the position, orientation, and surface temperature of the simulated northern front of the cold tongue varied during two years: 2000 (a strong La Niña year) and 2002 (a weak El Niño year) along 140°W. The black dots in Fig. 3 show the origin of the frontal coordinate system (θ_c) as a function of time. Note that TAO cruises were always conducted along meridians (e.g., north–south transects). Thus, our frontal coordinate system is not a "cross frontal"

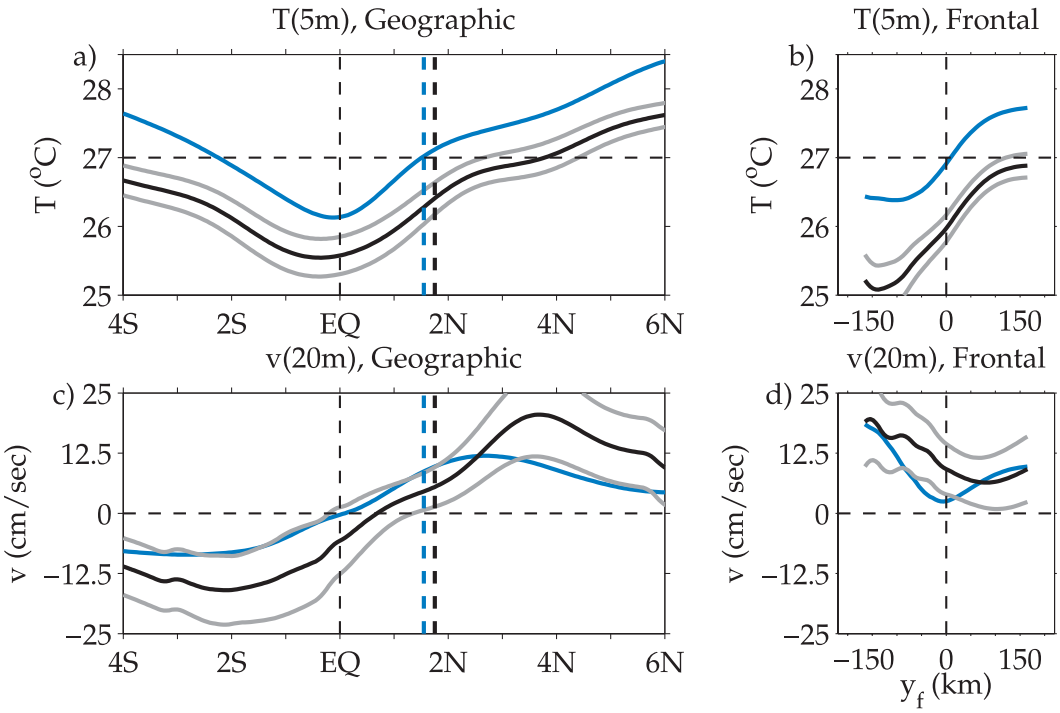

FIG. 4. Zonally and temporally averaged near-surface (a),(b) temperature and (c),(d) meridional currents obtained from shipboard ADCP (thick black line) and model (thick blue line) in geographic and frontal coordinates. Light gray lines represent standard errors for observed means. (left) Thick black and blue dashed line denotes the mean position of the observed and model front.

coordinate system (perpendicular to orientation of the instantaneous front) but rather its projection onto the meridional direction.

During the passage of a TIW, the northern front of the cold tongue can be highly convoluted. To focus on processes associated with the northern front of the cold tongue, fields were only analyzed within ±1.5° latitude (or ±165 km) of the front and data south of the equator were excluded from the analysis. Three transects were discarded because θ_c was located just south of the equator (this occurred twice along 140°W and once along 125°W). In the unusual instance of a double cold tongue minimum (two possible choices for θ_1), the northern value of θ_1 was chosen (this occurred once along each meridian).

Similar processing was applied to fields from the 9-yr model simulation (section 2b). Because model fields were continuous (no spatial gaps), they were linearly interpolated onto the 0.05° latitude grid. Model fields along 140° and 125°W were translated into frontal coordinates as outlined above for shipboard measurements. Less than 1% of the model time series was excluded from the frontal mean calculation because the center of the cold tongue was located south of the equator.

For the observed means, all error bars reported in this paper were computed via the delete-one jackknife scheme (Efron 1982) implemented by JMF01. This scheme calculates the standard error of an arithmetic mean and provides an estimate of how sensitive a mean is to removing one section (i.e., sampling error). This jackknife scheme assumes unbiased sampling and supplies a measure of the uncertainty associated with the small sample size. It does not, however, account for the systematic seasonal biases outlined in section 3a.

4. Geographic and frontal means

In this section, the (y, z) structure of zonally and temporally averaged temperature, horizontal currents, divergence of meridional flow (hereafter called meridional divergence), and vertical currents are all described. A comparison is made of observed and simulated means in both geographic and frontal coordinates. Note, coordinate transformation and computations are completed for each individual transect prior to zonal and temporal averaging (see section 3). The meridional structure of the geographic means is evaluated as a function of latitude, and the structure of the frontal means is evaluated as a function of meridional distance from the front (labeled y_f). In figures comparing geographic and frontal means, the abscissa scale is preserved (width of 1° latitude on

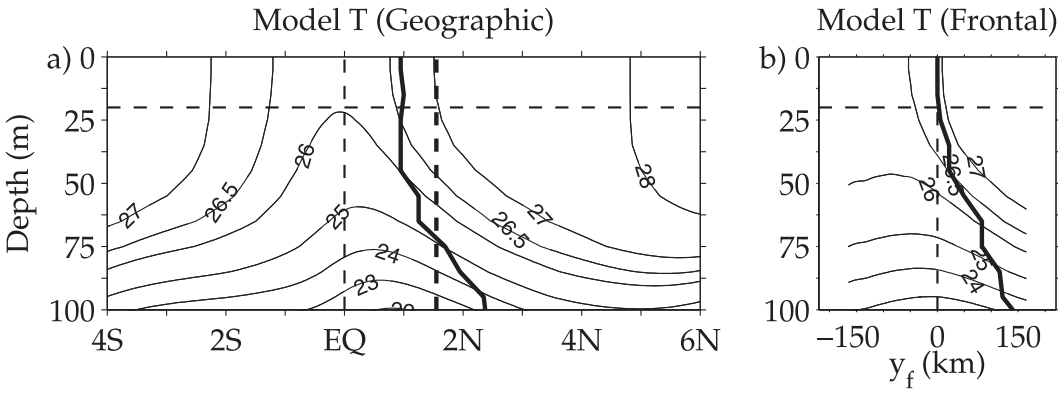

FIG. 5. Model (y, z) structure of mean temperature. Zonally and temporally averaged means are compared in (a) geographic and (b) frontal coordinates. Contour intervals are 1°C (with additional 26.5°C contour). (left) Thick dashed line denotes the mean position of the front. Thick solid lines correspond to the maximum mean temperature gradient as a function of depth.

left panels equals the width of 110 km on right panels) to allow for direct comparisons, and mean fields have been smoothed with a 0.5° latitude (approximately 60 km) triangle filter. The filter is applied to smooth small discontinuities that result from changes in sample size (e.g., there are more data north of equator than south of equator).

a. Temperature

Figures 4a,b compare the mean near-surface ADCP transducer (thick black line) and model 5-m (thick blue line) temperature across the cold tongue. Light gray lines denote sampling error bars (section 3b). In geographic coordinates (Fig. 4a), the observed cold tongue minimum has a mean value of 25.5° ± 0.3°C at 0.35°S and the mean position of the northern front of the cold tongue is at 1.76° ± 0.22°N. The model cold tongue minimum has a mean value of 26.1°C at 0.15°S, and the mean front is at 1.55°N. The meridional temperature gradients are similar, but the simulated profile is shifted by approximately 0.8°C. The fall and interannual sampling biases described in section 3a are largely responsible for the model–data temperature bias, although systematic model biases may also contribute to these temperature differences. The model–data temperature bias increases from 0.8° to 1.0°C when temperatures are averaged in frontal coordinates, consistent with the exclusion of the four El Niño transects. As expected, averaging in frontal coordinates sharpens the mean observed and model temperature gradients across the front to approximately 1.1°C over 100-km distance (Fig. 4b). Although frontal gradients can be as large as 3°C over 100-km distance during some cruises, the real strength of the front may still be underestimated because of meridional and temporal smoothing applied to the shipboard data.

Analysis of the mean (y, z) structure of the model temperature in both geographic and frontal coordinates (Fig. 5) reveals how temperature varies with depth near the northern front of the cold tongue. In geographic coordinates, the latitude of the maximum mean meridional temperature gradient does not match the mean position of the front (cf. thick line and thick dashed line in Fig. 5a), consistent with the presence of nonlinear frontal processes. In frontal coordinates, however, the location of the maximum mean meridional temperature gradient as a function of depth exactly matches the mean front computed from 5-m temperature in the upper 25 m (thick line in Fig. 5b lies at origin). Although the simulated front does not tilt with depth throughout most of the surface mixed layer, the latitude of its maximum temperature gradient in frontal coordinates moves poleward with depth between 25- and 100-m depth at an approximate rate of 18 km every 10 m. This tilt of the model front with depth is also found in the mean (y, z) structure of the density (not shown). Because shipboard measurements are only available at 5-m depth, a similar observational picture cannot be made. Nevertheless, we will show evidence in the following sections that suggests the observed front also tilts with depth.

b. Zonal currents

Although the TCs are described along a (y, z) transect, the TCs are not two-dimensional cells and are embedded in strong westward and eastward flows. Figure 6 shows the extent to which the mean structure of the zonal currents differ in geographic and frontal coordinates. When averaged in geographic coordinates, the eastward-flowing Equatorial Undercurrent and North Equatorial Countercurrent and the southern and northern branches of the westward-flowing South Equatorial Current are well reproduced by both the ADCP measurements and the model (left panels of Fig. 6) when compared with previous observational studies (JMF01;

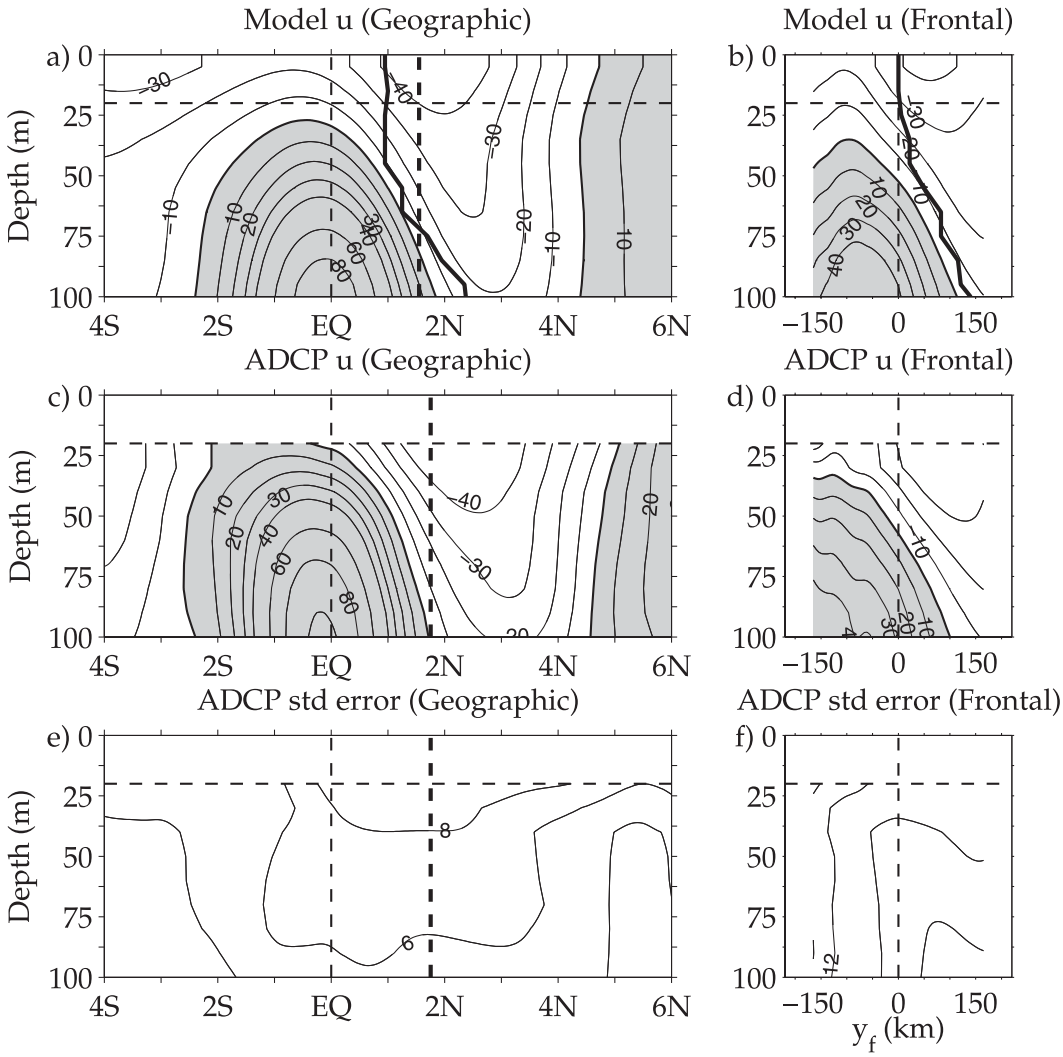

FIG. 6. The (y, z) structure of the mean zonal currents obtained from (a),(b) model and (c),(d) shipboard ADCP. (a)–(d) compare zonally and temporally averaged currents in (left) geographic and (right) frontal coordinates. (e),(f) Standard errors for the observed means are shown. Contour intervals are 10 cm s^{-1} between ±40 and 20 cm s^{-1} otherwise, and shaded contours indicate positive values in (a)–(d). Contour intervals are 2 cm s^{-1} in (e),(f). Thick dashed line in (left) denotes the mean position of the front. Thick solid line in (a)–(b) corresponds to maximum mean temperature gradient from Fig. 5.

Johnson et al. 2002). When averaged in frontal coordinates, the zonal currents are weakened and widened (right panels of Fig. 6). Below 25 m, the boundary between the Equatorial Undercurrent and north branch of the South Equatorial Current tilts with depth (Figs. 6b,d) and follows the tilt of the model front (thick line in Fig. 6b).

c. *Meridional currents*

Mean meridional flow in the surface limb of the TCs is much weaker than the observed flow during the passage of a TIW (Figs. 4c,d; Kessler et al. 1998; Weisberg and Qiao 2000; CK09), and the large sampling errors (on average 7 cm s^{-1}) reflect the uncertainty associated with aliased TIWs. In geographic coordinates, both ADCP and model meridional currents at 20 m (thick black and blue lines in Fig. 4c, respectively) exhibit mean poleward flow (equatorial divergence). Northward currents increase across the mean position of the northern front (thick dashed lines in Fig. 4c) with a local maximum in northward flow 1°–2° latitude north of the mean front (20.5 ± 8.7 cm s^{-1} at 3.7°N in the observations; 12.0 cm s^{-1} at 2.7°N in the model). There is no apparent trace of a secondary circulation near the mean position of the northern front. South of the equator, the southward flow is strongest at 2.1°S in the observations (−16.0 ± 7.1 cm s^{-1}) and at 2.8°S in the model (−8.6 cm s^{-1}). The

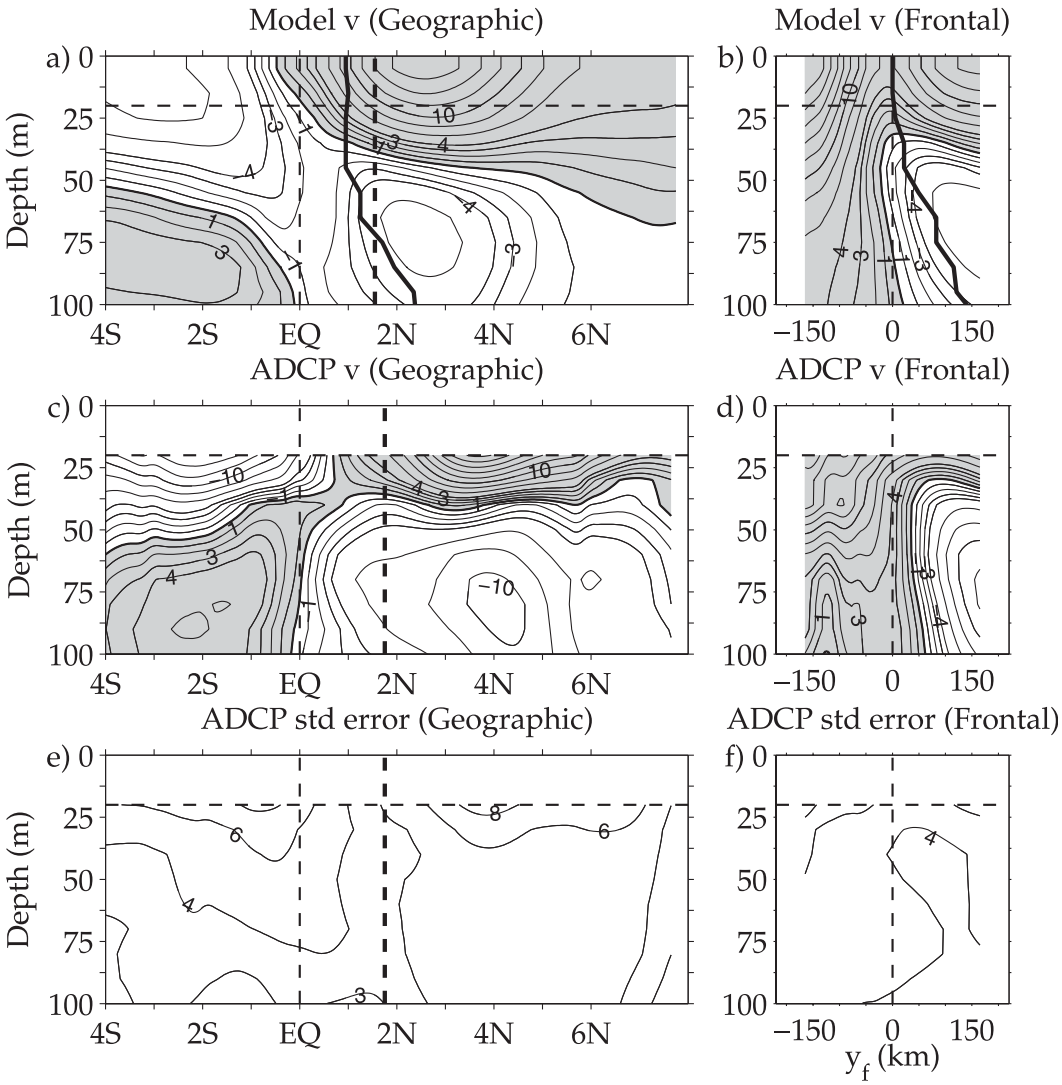

FIG. 7. As in Fig. 6, but for mean meridional currents. Contour intervals are 1 cm s^{-1} between ±4 and 2 cm s^{-1} otherwise, and shaded contours indicate positive values in (a)–(d).

observed currents are much stronger than the simulated currents, but both exhibit similar equatorial asymmetry, with a ratio of the magnitude of maximum northward flow to maximum southward flow of 1.28 in the observations and 1.39 in the model.

The mean (y, z) structure of meridional flow in geographic coordinates is similar to the structure described by previous observations, with two notable differences (cf. Fig. 5 of JMF01 with Fig. 7c). The magnitude of the observed meridional currents in the central equatorial Pacific are stronger (this difference is accentuated if currents are vertically extrapolated to the surface using vertical shear at 20 m), and there is equatorially asymmetric equatorward flow in the subsurface limb. Below the surface limb, the observed maximum southward flow (11.1 ± 5.6 cm s^{-1} at 4.1°N and 80-m depth) is 1.73 times faster than the maximum northward flow (6.4 ± 3.5 cm s^{-1} at 2.3°S and 90-m depth). The model exhibits similar asymmetry with a ratio of 1.88 (Fig. 7a). In contrast, the JMF01 values in Fig. 1 give a ratio of 0.8. These differences are primarily due to the narrower zonal-averaging window (ratio reduces to 1.04 when all available ADCP data are averaged between 170° and 95°W) and are secondarily due to the longer ADCP record used in this study (ratio further reduces to 0.75 when a second decade of data is excluded). Despite considerable sampling errors (Fig. 7e), the observed equatorial asymmetry described here is consistent with previous simulations of central equatorial Pacific circulation (e.g., Kessler et al. 1998; Brown et al. 2007b; Perez and Kessler 2009).

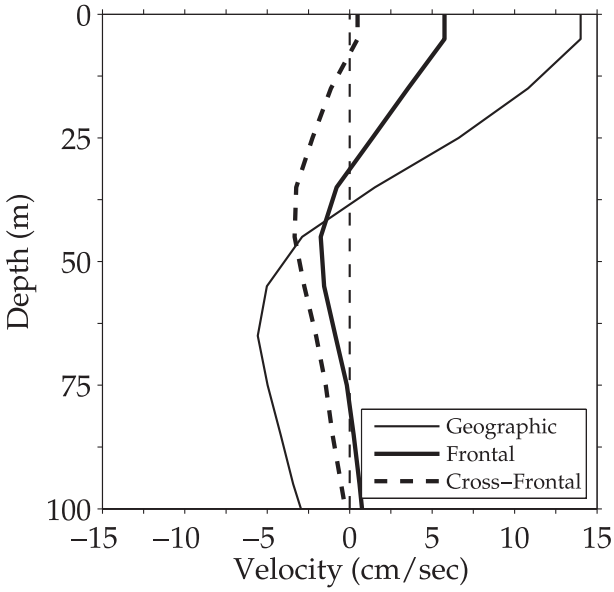

FIG. 8. A comparison of model mean currents at the front as a function of depth. Thin solid line corresponds to meridional flow averaged in geographic coordinates at $\theta = \overline{\theta}_c$ (mean position of front). Thick solid line corresponds to meridional flow averaged in frontal coordinates at $y_f = 0$. Thick dashed line corresponds to cross-frontal flow averaged in frontal coordinates at $y_f = 0$. Cross-frontal flow is defined as $v_n = v \cos \alpha - u \sin \alpha$, where u and v are the zonal and meridional currents at the front and α is angle of front relative to due east.

When averaged in frontal coordinates, the mean meridional flow at 20 m has a pronounced local minimum in the northward flow (convergent flow) near the mean position of the front (thick black and blue lines in Fig. 4d). This convergence occurs in both observations and model, but the structure differs with minimum northward flow 82.5 km north of the surface front in the observations and 5.5 km south of the surface front in the model. This minimum in northward flow spans the upper 30 m of the water column in the model (Fig. 7b) and is present between 20 and 30 m in the observations (Fig. 7d). Moreover, frontal averaging brings out a surprising new feature not seen in the geographic means: strong subsurface convergent flow below 30-m depth that is centered approximately 40 km north of the surface front in the observations and a few kilometers south of the front in the model (Figs. 7b,d). The convergent flow near the front will be discussed in more detail in the following sections.

Note that, in a true cross-frontal coordinate system (perpendicular to orientation of the instantaneous front), we would expect no mean flow across the front. When model velocities are averaged in cross-frontal coordinates, the mean near-surface, cross-frontal flow is near zero, 0.6 cm s^{-1} (cf. thick dashed and thick solid lines in Fig. 8), and the secondary circulation is more apparent. TAO cruises were always conducted along north–south transects; thus, it was not possible to conduct a model–data comparison of the circulation in true cross-frontal coordinates.

d. Meridional divergence

We now discuss the mean (y, z) structure of meridional divergence (Fig. 9). In geographic coordinates, there is mean divergence in the surface limb of the TCs between roughly 2.0°S and 3.7°N in the observations and 3.1°S and 2.6°N in the model, with mean convergence beneath (left panels of Fig. 9). In frontal coordinates, however, there is mean meridional convergence below 20-m depth near the northern front of the cold tongue, bounded on the north and south by regions of divergence (right panels of Fig. 9). This strong convergence extends to the surface in the model, with a 71.5-km southward shift in the surface mixed layer so that, at the surface, the mean convergent flow lies just south of the surface front (Fig. 9b). The poleward shift of the maximum convergence with increasing depth mirrors the depth dependence of the model front (maximum mean temperature gradient given by the thick line in Fig. 9b). Although observations are not available to make this same comparison, we note that the observed location of maximum convergence also moves poleward with depth (Fig. 9d). This, combined with structure of the zonal currents (Fig. 6d), suggests that the observed front also tilts with depth.

e. Vertical currents

The vertical component of velocity can be estimated by vertically integrating the divergence of the horizontal flow, $\partial w/\partial z = -(\partial u/\partial x + \partial v/\partial y)$. Computing the divergence of the zonal flow from quasi-synoptic cruise transects along 140° and 125°W would alias TIWs. Therefore, the divergence of zonal currents (hereafter called zonal divergence) is neglected, and $\partial w/\partial z \approx -\partial v/\partial y$ is used to estimate vertical currents. Instantaneously, the zonal divergence can be large, and the suitability of this assumption will be addressed later in this section. Note, estimating vertical currents from shipboard ADCP requires the additional step of extrapolating the meridional divergence in the upper 20 m using vertical shear at 20 m as in JMF01. Although this linear extrapolation is overly simplistic near the northern front of the cold tongue (CK09), we only do so here to allow for qualitative comparison with the model and previous observations (JMF01).

The structure of the vertical currents (as estimated from meridional divergence) is complex with several distinct equatorial upwelling and off-equatorial downwelling maxima present in both observed and model geographic

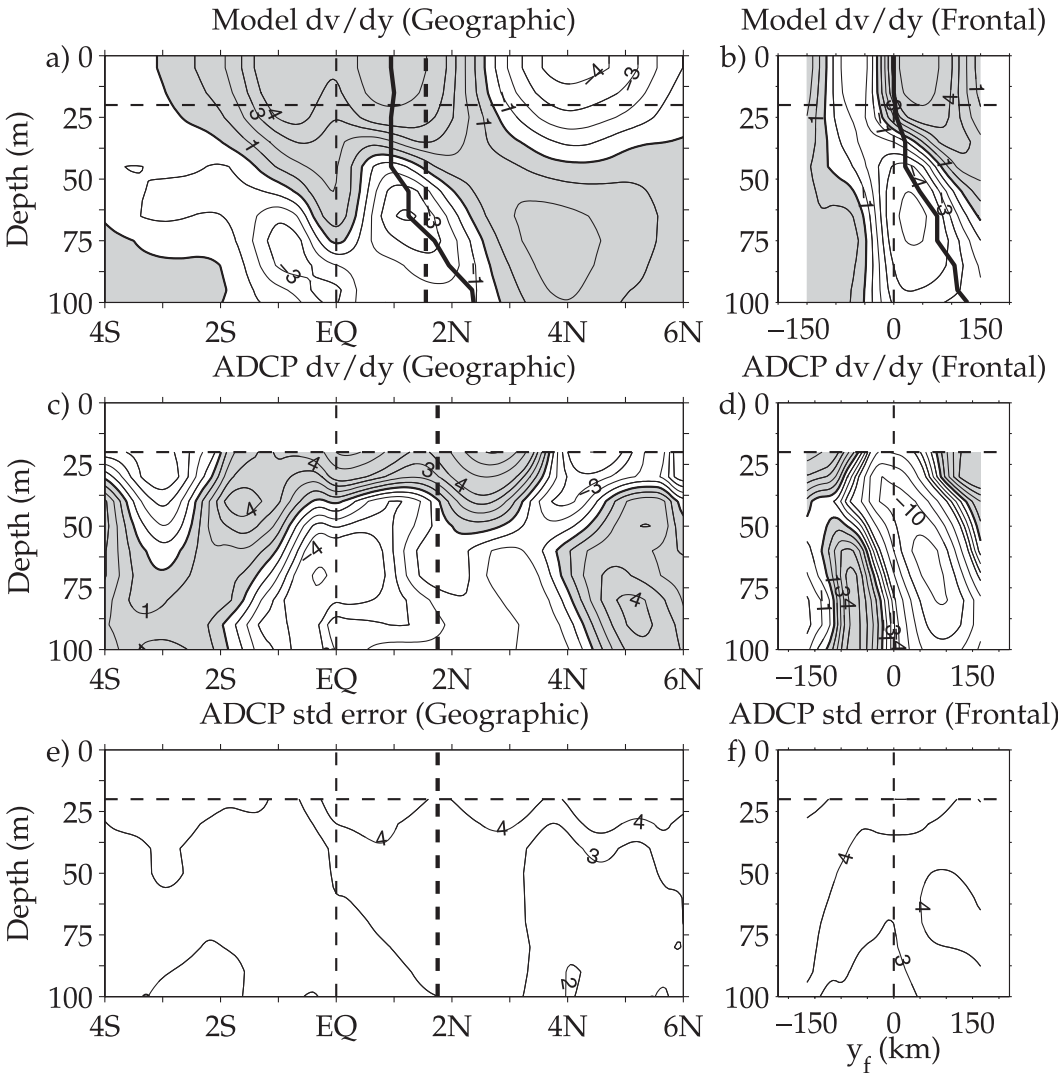

FIG. 9. As in Fig. 6, but for mean meridional divergence. Contour intervals are 1×10^{-6} s^{-1} between $\pm 4 \times 10^{-6}$ and 2×10^{-6} s^{-1} otherwise, and shaded contours indicate positive values in (a)–(d).

means (Figs. 10a,c). The observed upwelling maxima (2.9 ± 1.6 m day^{-1} at 0.15°N and 40-m depth and 3.7 ± 2 m day^{-1} at 2.7°N and 50-m depth) are centered about the mean position of the front rather than the equator as is the case in the model (Figs. 10a,c). The observed off-equatorial downwelling is separated into several narrow maxima with values on the order of -2 m day^{-1} centered at 5°S, 3.1°S, 4.4°N, and 6.2°N (Fig. 10c); however, given the large sampling errors, these narrow maxima may not be distinct features (Fig. 10e). In contrast, the model has broad regions of off-equatorial downwelling between 3° and 8° latitude, with maxima near 4° latitude (Fig. 10a). JMF01 did find a complicated vertical flow structure, but significant downwelling was only reported near 8.0°N. The absence of strong downwelling near 4.0°N in their study is a consequence of the large zonal-averaging window (170°–95°W) and shorter data record.

In frontal coordinates, the estimated mean vertical currents from ADCP data exhibit downwelling directly at the front in the surface mixed layer that increases in magnitude and tilts poleward with depth (Fig. 10d) because of the strong frontal convergence described in section 4d (Fig. 9d). The simulated downwelling has a similar vertical structure but is shifted 70 km south of the front in the surface mixed layer (Fig. 10b) and differs in magnitude (e.g., at 50-m depth, observed maximum downwelling is -2.8 ± 2.4 m day^{-1} and model maximum downwelling is -1.0 m day^{-1}). In both the observations and model, the downwelling near the front is bounded to the north and south by regions of strong

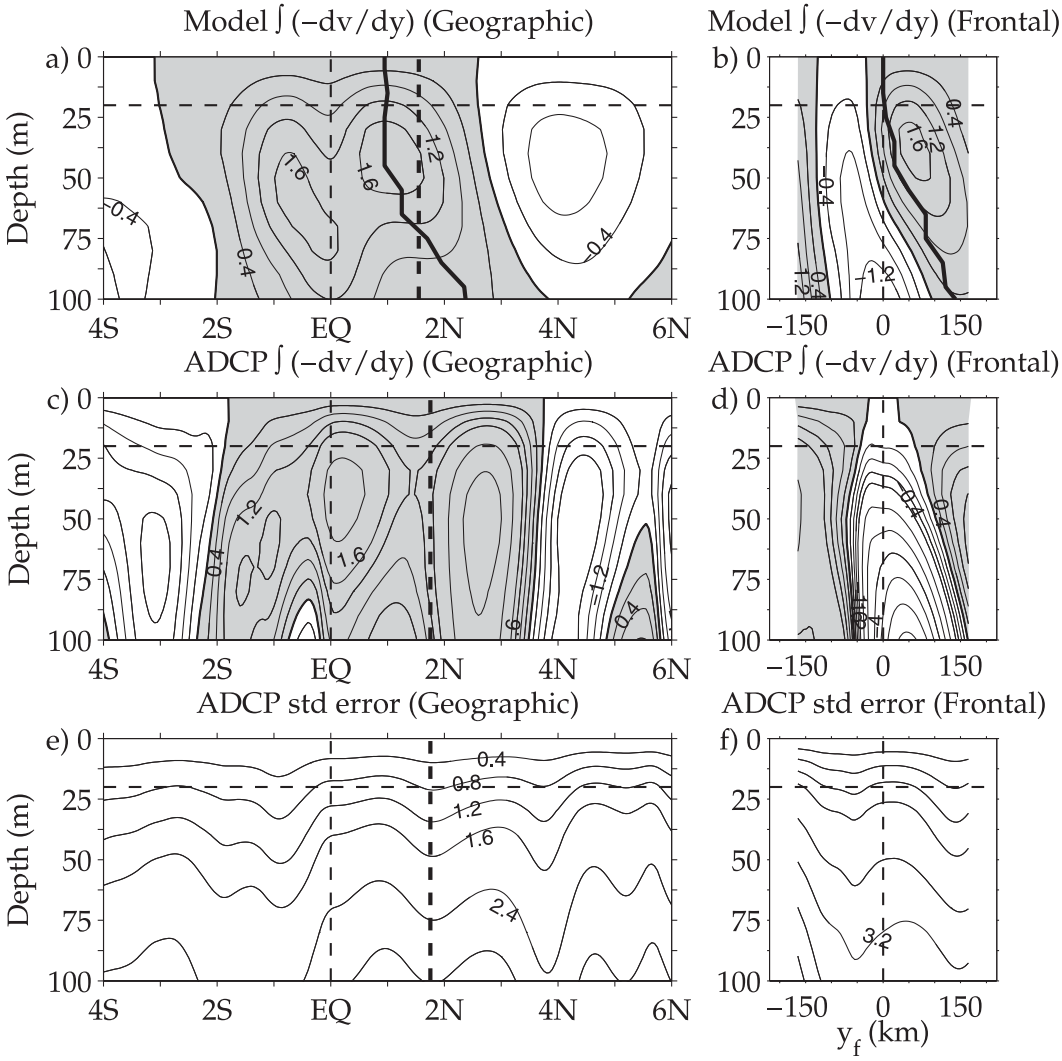

FIG. 10. As in Fig. 6, but for mean vertical currents estimated by vertically integrating meridional divergence. Contour intervals are 0.4 m day^{-1} between ±1.6 and 0.8 m day^{-1} otherwise, and shaded contours indicate positive values in (a)–(d). The errors are small above 20 m, because they do not reflect the uncertainty introduced by the vertical extrapolation of ADCP data above 20 m.

upwelling consistent with the divergent flow shown in Figs. 9b,d.

Figure 11a shows that in the model the mean impact of neglecting zonal divergence is very small in geographic coordinates (consistent with Johnson 2001; JMF01; Perez and Kessler 2009). Although when averaged in frontal coordinates, there are differences between true vertical currents and those estimated from meridional divergence (e.g., downwelling and upwelling do not grow unbounded with depth but rather have broad maxima near 40-m depth, and there is no zone of upwelling south of the front), the essential behavior at the front is unchanged (cf. Figs. 10b, 11b). In other words, we can expect that the mean impact of neglecting zonal divergence in estimates of the vertical currents from ADCP data will not change the overall structure of the flow at the front.

Thus, both the observations and model provide evidence of a coherent mean quasi-adiabatic secondary circulation with cold tongue water moving northward toward the front in the surface mixed layer (label 1 in Fig. 11d). The cold water cannot move across the front, so it is downwelled just south of the front. North of the front, water below the surface mixed layer moves southward toward the front and upwells following the tilt of the maximum mean temperature gradient (label 2 in Fig. 11d). Because of forcing by the trade winds, there must be poleward Ekman flow in the surface mixed layer and, north of the front, the newly upwelled water flows

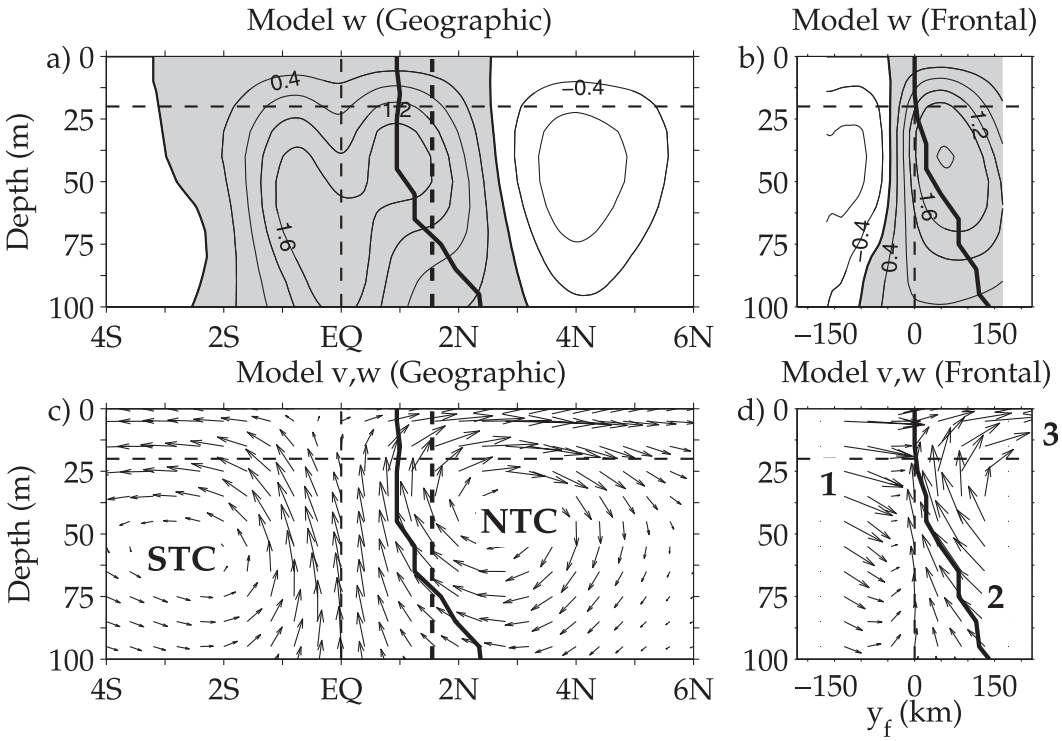

FIG. 11. Model (y, z) structure of mean meridional and vertical currents in (left) geographic and (right) frontal coordinates. Shown are (a),(b) mean vertical currents with same contour intervals used in Fig. 10 and (c),(d) mean velocity vectors. The thick dashed line in (left) denotes the mean position of the front. The thick solid line corresponds to maximum mean temperature gradient from Fig. 5. STC and NTC are identified. Labels 1, 2, and 3 identify components of the secondary circulation associated with the front (as described in section 4e). Vectors are plotted every 0.4° latitude (approximately 40 km).

northward satisfying that constraint (label 3 in Fig. 11d). This mean secondary circulation, however, should not be considered as a frozen field that migrates with the front. As we will show in the next section, there is significant variability in the meridional and vertical motion near the front associated with TIWs.

f. The role of TIWs

The relationship between TIWs and the frontal secondary circulation can be fully explored in the model and used to interpret the sparse shipboard observations. The mean frontal circulation depicted in Fig. 11d is manifest when averaged over many TIWs and seasons but is not always present at the instantaneous front. The quasi-adiabatic frontal circulation is strongest when the front is strongest and thus when TIWs are strongest, and it is highly dependent on the phase of the TIWs (Figs. 3a, 12). For example, during one TIW cycle (identified by sequence of yellow lines in Fig. 3a), there was southward-upwelling flow on the warm side of the front (Figs. 12a,b), followed 8 days later by northward-downwelling flow on the cold side of the front (Figs. 12c,d), another 8 days later by general upwelling (Figs. 12e,f), and 8 days after that by a circulation pattern similar to the mean frontal circulation (Figs. 12g,h). Note that, in all of these cases, the flow tends to slide along sloping isotherms. Instances of convergent flow and downwelling on the cold side of the front in the leading edge of a TIW cusp and divergent flow and upwelling on the cold side of the front in the trailing edge of a TIW cusp have been previously documented in other observational and numerical studies for individual TIWs and associated TIVs (Philander et al. 1986; Flament et al. 1996; Johnson 1996, Kennan and Flament 2000; Menkes et al. 2002, 2006; Dutrieux et al. 2008) and in and of itself is not a new result. What this study does demonstrate is that, when the model is averaged over many TIWs and seasons, the vertical and meridional motions associated with these waves and vortices lead to the nonzero mean frontal circulation given by Fig. 11d with net convergent flow and downwelling on the cold side of the front. Because of the large meridional displacements of the northern front associated with TIWs, the downwelling on the cold side of the front on a given day can occur at the same latitude as upwelling on the warm side of the front a few days later. Thus, when averaged in geographic coordinates, there is no

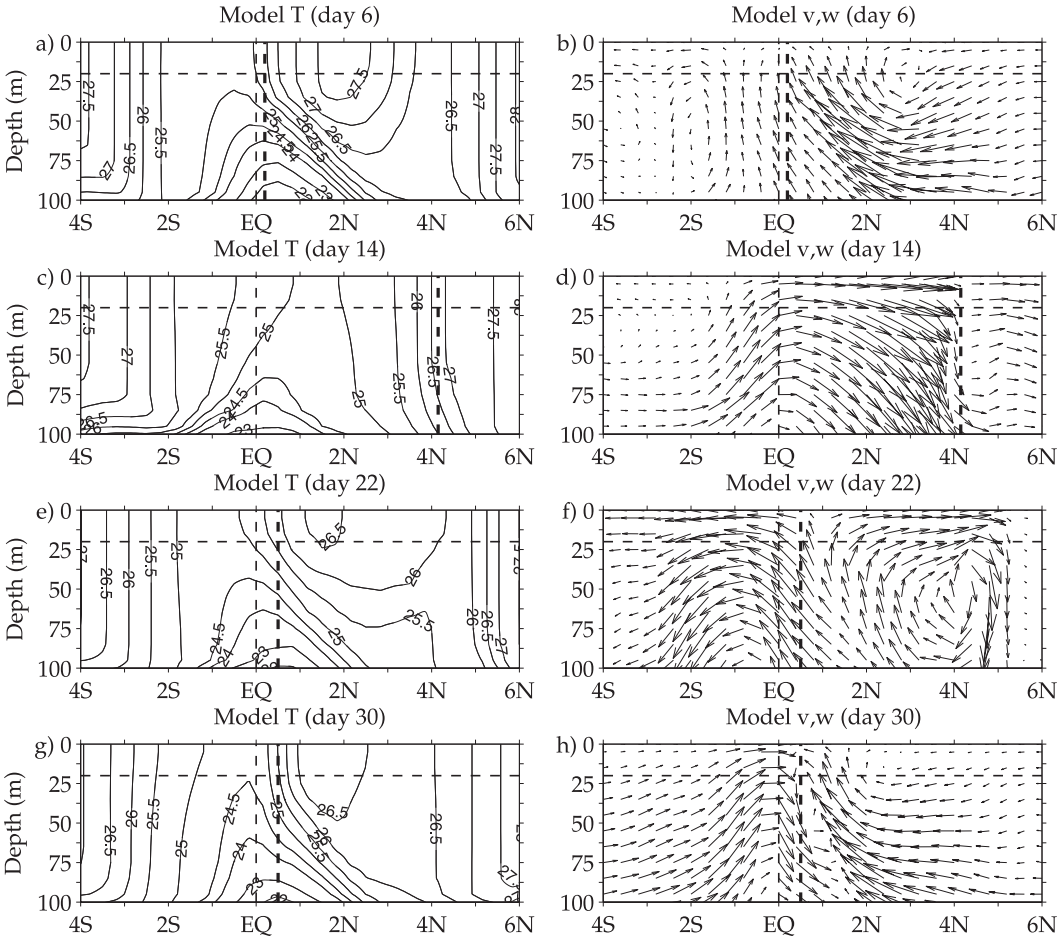

FIG. 12. Model (y, z) structure of temperature and meridional and vertical currents along 140°W for select days in January 2000 (see yellow lines in Fig. 3a): (a),(b) convergent front on day 6; (c),(d) convergent front on day 14; (e),(f) divergent front on day 22; and (g),(h) convergent front on day 30. Thick dashed lines denote the position of the front. (left) Contour intervals are 1°C (with additional 26.5°C contour). (right) Vectors are plotted every 0.4° latitude.

apparent quasi-adiabatic secondary circulation associated with the mean front.

5. Discussion

TAO shipboard ADCP measurements were used to describe the mean structure of the shallow meridional–vertical TCs in the central equatorial Pacific and in particular to investigate the secondary circulation associated with the northern front of the cold tongue. Because the front can meander over several degrees during the passage of a TIW, the mean flow is analyzed in both geographic coordinates and a coordinate system centered on the instantaneous position of the front. This offers an alternative means to visualize the quasi-adiabatic flow that complements previous isopycnal coordinate analyses (Hazeleger et al. 2001; Brown et al. 2007b; Richards et al. 2009) and can be readily applied to upper-ocean cross-equatorial transects of temperature and velocity. Results from a 9-yr tropical Pacific model simulation were used to provide context for the observed results.

When averaged in frontal coordinates, the measurements show a near-surface minimum in northward flow north of the surface front, with maximum convergence of the meridional flow slightly equatorward of the front. This region of convergent flow and downwelling (inferred from vertical integration of meridional divergence) extends below the surface mixed layer, tilts poleward with depth, and is meridionally bounded by regions of divergence and upwelling. Similarly, the model shows that, on average, surface cold tongue water moves northward toward the frontal region and dives below tilted front, whereas subsurface water north of the front moves southward toward the front, upwells, and then moves northward in the surface mixed layer. The model also demonstrates that this mean quasi-adiabatic secondary

circulation is not a frozen field that migrates with the front but is instead highly dependent on the phase of the TIWs: southward-upwelling flow on the warm side of the front tends to occur when the front is displaced southward, whereas northward-downwelling flow on the cold side of the front occurs when the front is displaced northward. Consequently, the mean geographic sections show little trace of a quasi-adiabatic secondary circulation near the mean front (i.e., on average, cold northward-moving water does not appear to slide under the warmer water to the north, and corresponding upwelling on the northern side of the front is not visible in the Eulerian average). Instead, when averaged in geographic coordinates, the observed and simulated TCs appear to be equatorially asymmetric with larger meridional currents north of the equator that increase in magnitude across the mean position of the front. This flow that appears to cross the mean front, however, must be considered as a rectified mean flow. In fact, on average, parcels do not cross the front.

We have shown that TIWs fundamentally affect the meridional–vertical circulation near the front. Quasi-adiabatic slantwise motion is observed near the front during TIWs, but it is not manifest when averaged in geographic coordinates. The dynamics that produce the slantwise motion (e.g., baroclinic instability, symmetric instability, and Ekman frontal processes) have not been diagnosed. These motions, however, greatly impact the mean equatorial Pacific cold tongue heat balance. Previous studies have shown that advection by the TIWs warms the surface cold tongue waters, whereas advection by the mean and seasonal circulation cools the surface cold tongue waters (Wyrtki 1981; Hansen and Paul 1984; Bryden and Brady 1989; Baturin and Niiler 1997; Swenson and Hansen 1999; Wang and McPhaden 1999, 2000; Jochum et al. 2007). The present study demonstrates that the near-surface circulation is fundamentally affected by the front; however, direct measurements in the layer above 40 m are relatively rare. Thus, further work is needed to resolve how heat advection by TIWs and the mean and seasonal circulation interact, especially near the front north of the equator.

This analysis could not have been conducted without the use of TAO shipboard ADCP measurements. Because they make vertical cross sections of the flow over many years, they are the only dataset from which the mean structure of the meridional circulation in the central equatorial Pacific can be studied. However, as of the year 2006, these observations do not resolve the structure of the currents above 40 m. Thus, for monitoring future changes in the TC, we highly recommend that ships that service the TAO array be enhanced to sample the near-surface layer.

Acknowledgments. The authors thank Greg Johnson and Chris Meinen for helpful discussion regarding the data analysis. We also thank Jules Hummon, Eric Firing, and Patrick Caldwell for providing data from the JASADCP archive. Comments from anonymous reviewers, Jaclyn Brown, Kelvin Richards, Eric Firing, Bob Molinari, and Sang-Ki Lee led to significant improvements in the paper. The authors were funded by NOAA/CPO, and this research was performed while RCP held an NRC Research Associateship Award at NOAA/PMEL.

REFERENCES

Baturin, N. G., and P. P. Niiler, 1997: Effects of instability waves in the mixed layer of the equatorial Pacific. *J. Geophys. Res.,* **102,** 27 771–27 793.

Bretherton, F. P., R. E. Davis, and C. B. Fandry, 1976: A technique for objective analysis and design of oceanographic measurements applied to MODE-73. *Deep-Sea Res.,* **23,** 559–582.

Brown, J. N., J. S. Godfrey, and R. Fiedler, 2007a: A zonal momentum balance on density layers for the central and eastern equatorial Pacific. *J. Phys. Oceanogr.,* **37,** 1939–1955.

——, ——, and A. Schiller, 2007b: A discussion of flow pathways in the central and eastern equatorial Pacific. *J. Phys. Oceanogr.,* **37,** 1321–1339.

Bryden, H., and E. C. Brady, 1989: Eddy momentum and heat fluxes and their effects on the circulation of the equatorial Pacific Ocean. *J. Mar. Res.,* **47,** 55–79.

Contreras, R. F., 2002: Long-term observations of tropical instability waves. *J. Phys. Oceanogr.,* **32,** 2715–2722.

Cronin, M. F., and W. S. Kessler, 2009: Near-surface shear flow in the tropical Pacific cold tongue front. *J. Phys. Oceanogr.,* **39,** 1200–1215.

Deser, C. S., and J. M. Wallace, 1990: Large-scale atmospheric circulation features of warm and cold episodes in the tropical Pacific. *J. Climate,* **3,** 1254–1281.

Dutrieux, P., C. E. Menkes, J. Vialard, P. Flament, and B. Blanke, 2008: Lagrangian study of tropical instability vortices in the Atlantic. *J. Phys. Oceanogr.,* **38,** 400–417.

Efron, B., 1982: *The Jackknife, the Bootstrap, and Other Resampling Plans*. CBMS-NSF Regional Conference Series in Applied Mathematics, Vol. 38, SIAM, 92 pp.

Flament, P., S. C. Kennan, R. A. Knox, P. P. Niiler, and R. L. Bernstein, 1996: The three-dimensional structure of an upper ocean vortex in the tropical Pacific Ocean. *Nature,* **383,** 610–613.

Garrett, C. J. R., and J. W. Loder, 1981: Dynamical aspects of shallow sea fronts. *Philos. Trans. Roy. Soc. London,* **302A,** 563–581.

Griffies, S. M., M. J. Harrison, R. C. Pacanowski, and A. Rosati, 2003: A technical guide to MOM4. NOAA/GFDL Ocean Group Tech. Rep. 5, 295 pp.

Haine, T. W. N., and J. Marshall, 1998: Gravitational, symmetric, and baroclinic instability of the ocean mixed layer. *J. Phys. Oceanogr.,* **28,** 634–658.

Hansen, D. V., and C. A. Paul, 1984: Genesis and effects of long waves in the equatorial Pacific. *J. Geophys. Res.,* **89,** 10 431–10 440.

Hazeleger, W., P. de Vries, and G. J. van Oldenborgh, 2001: Do tropical cells ventilate the Indo-Pacific equatorial thermocline? *Geophys. Res. Lett.,* **28,** 1763–1766.

Izumo, T., 2005: The equatorial undercurrent, meridional overturning circulation, and their roles in mass and heat exchanges

during El Niño events in the tropical Pacific Ocean. *Ocean Dyn.,* **55,** 110–123.

Jochum, M., and R. Murtugudde, 2006: Temperature advection by tropical instability waves. *J. Phys. Oceanogr.,* **36,** 592–605.

——, M. F. Cronin, W. S. Kessler, and D. Shea, 2007: Observed horizontal temperature advection by tropical instability waves. *Geophys. Res. Lett.,* **34,** L09604, doi:10.1029/2007GL029416.

Johnson, E. S., 1996: A convergent instability wave front in the central tropical Pacific. *Deep-Sea Res. II,* **43,** 753–778.

——, and P. E. Plimpton, 1999: TOGA/TAO shipboard ADCP data report, 1991–1995. NOAA Data Rep. ERL PMEL-67, 23 pp.

Johnson, G. C., 2001: The Pacific Ocean subtropical cell surface limb. *Geophys. Res. Lett.,* **28,** 1771–1774.

——, M. J. McPhaden, and E. Firing, 2001: Equatorial Pacific Ocean horizontal velocity, divergence, and upwelling. *J. Phys. Oceanogr.,* **31,** 839–849.

——, B. M. Sloyan, W. S. Kessler, and K. E. McTaggart, 2002: Direct measurements of upper ocean currents and water properties across the tropical Pacific Ocean during the 1990s. *Prog. Oceanogr.,* **52,** 31–61.

Kennan, S. C., and P. J. Flament, 2000: Observations of a tropical instability vortex. *J. Phys. Oceanogr.,* **30,** 2277–2301.

Kessler, W. S., L. M. Rothstein, and D. Chen, 1998: The annual cycle of SST in the eastern tropical Pacific, diagnosed in an ocean GCM. *J. Climate,* **11,** 777–799.

Kummerow, C., W. Barnes, T. Kozu, J. Shiue, and J. Simpson, 1998: The Tropical Rainfall Measuring Mission (TRMM) sensor package. *J. Atmos. Oceanic Technol.,* **15,** 808–816.

Legeckis, R., 1977: Long waves in the equatorial Pacific Ocean: A view from a geostationary satellite. *Science,* **197,** 1179–1181.

Lu, P., J. P. McCreary, and B. A. Klinger, 1998: Meridional circulation cells and the source waters of the Pacific equatorial undercurrent. *J. Phys. Oceanogr.,* **28,** 62–84.

Lyman, J. M., G. C. Johnson, and W. S. Kessler, 2007: Distinct 17- and 33-day tropical instability waves in subsurface observations. *J. Phys. Oceanogr.,* **37,** 855–872.

McCreary, J. P., 1981: A linear stratified ocean model of the equatorial undercurrent. *Philos. Trans. Roy. Soc. London,* **298A,** 603–635.

——, and P. Lu, 1994: Interaction between the subtropical and equatorial ocean circulations: The subtropical cell. *J. Phys. Oceanogr.,* **24,** 466–497.

Menkes, C. E., and Coauthors, 2002: A whirling ecosystem in the equatorial Atlantic. *Geophys. Res. Lett.,* **29,** 1553, doi:10.1029/2001GL014576.

——, J. G. Vialard, S. C. Kennan, J.-P. Boulanger, and G. V. Madec, 2006: A modeling study of the impact of tropical instability waves on the heat budget of the eastern equatorial Pacific. *J. Phys. Oceanogr.,* **36,** 847–865.

Mitchell, T. P., and J. M. Wallace, 1992: The annual cycle in equatorial convection and sea surface temperature. *J. Climate,* **5,** 1140–1156.

Perez, R. C., and W. S. Kessler, 2009: The three-dimensional structure of tropical cells in the central equatorial Pacific Ocean. *J. Phys. Oceanogr.,* **39,** 27–49.

Philander, S. G. H., W. J. Hurlin, and R. C. Pacanowski, 1986: Properties of long equatorial waves in models of the seasonal cycle in the tropical Atlantic and Pacific oceans. *J. Geophys. Res.,* **91,** 14 207–14 211.

——, ——, and A. D. Seigel, 1987: Simulation of the seasonal cycle of the tropical Pacific Ocean. *J. Phys. Oceanogr.,* **17,** 1986–2002.

Qiao, L., and R. H. Weisberg, 1995: Tropical instability wave kinematics: Observations from the Tropical Instability Wave Experiment. *J. Geophys. Res.,* **100,** 8677–8693.

Reynolds, R. W., T. M. Smith, C. Liu, D. B. Chelton, K. S. Casey, and M. G. Schlax, 2007: Daily high-resolution-blended analyses for sea surface temperature. *J. Climate,* **20,** 5473–5496.

Richards, K., S.-P. Xie, and T. Miyama, 2009: Vertical mixing in the ocean and its impact on the coupled ocean–atmosphere system in the eastern tropical Pacific. *J. Climate,* **22,** 3703–3719.

Risien, C. M., and D. B. Chelton, 2008: A global climatology of surface wind and wind stress fields from eight years of QuikSCAT scatterometer data. *J. Phys. Oceanogr.,* **38,** 2379–2413.

Straneo, F., M. Kawase, and S. C. Riser, 2002: Idealized models of slantwise convection in a baroclinic flow. *J. Phys. Oceanogr.,* **32,** 558–572.

Swenson, M. S., and D. V. Hansen, 1999: Tropical Pacific Ocean mixed layer heat budget: The Pacific cold tongue. *J. Phys. Oceanogr.,* **29,** 69–81.

Thomas, L., and R. Ferrari, 2008: Friction, frontogenesis, and the stratification of the surface mixed layer. *J. Phys. Oceanogr.,* **38,** 2501–2518.

Thompson, L., 2000: Ekman layers and two-dimensional frontogenesis in the upper ocean. *J. Geophys. Res.,* **105,** 6437–6451.

Wallace, J. M., T. P. Mitchell, and C. S. Deser, 1989: The influence of sea surface temperature on surface wind in the eastern equatorial Pacific: Seasonal and interannual variability. *J. Climate,* **2,** 1492–1499.

Wang, W., and M. J. McPhaden, 1999: The surface-layer heat balance in the equatorial Pacific Ocean. Part I: The mean seasonal cycle. *J. Phys. Oceanogr.,* **29,** 1812–1831.

——, and ——, 2000: The surface-layer heat balance in the equatorial Pacific Ocean. Part II: Interannual variability. *J. Phys. Oceanogr.,* **30,** 2989–3008.

Weisberg, R. H., and L. Qiao, 2000: Equatorial upwelling in the central Pacific estimated from moored velocity profilers. *J. Phys. Oceanogr.,* **30,** 105–124.

Wyrtki, K., 1981: An estimate of equatorial upwelling in the Pacific. *J. Phys. Oceanogr.,* **11,** 1205–1214.

Yu, L., and R. A. Weller, 2007: Objectively analyzed air–sea heat fluxes for the global ice-free oceans (1981–2005). *Bull. Amer. Meteor. Soc.,* **88,** 527–539.

——, ——, and B. Sun, 2004: Improving latent and sensible heat flux estimates for the Atlantic Ocean (1988–99) by a synthesis approach. *J. Climate,* **17,** 373–393.

Zhang, Y., W. B. Rossow, A. A. Lacis, V. Oinas, and M. I. Mishchenko, 2004: Calculation of radiative fluxes from the surface to top of atmosphere based on ISCCP and other global data sets: Refinements of the radiative transfer model and the input data. *J. Geophys. Res.,* **109,** D19105, doi:10.1029/2003JD004457.